

# Numerical analysis of shrinkage induced micro-cracking of concrete based on Peridynamic theory

Yudan. JIN<sup>1,a</sup>, Meng. WANG<sup>1,b</sup>, Yun. JIA<sup>1,c,\*</sup>, Jianfu, SHAO<sup>1,d</sup>

1. Univ. Lille, CNRS, Centrale Lille, FRE 2016-LaMcube-Laboratoire de Mécanique de Lille, multiphysique, multiéchelle, F-59000 Lille, France

a. yudan.jin.etu@univ-lille.fr

b. meng.wang.etu@univ-lille.fr

c,\*. yun.jia@univ-lille.fr

d. jian-fu.shao@polytech-lille.fr

## Résumé :

*Le présent travail consiste à présenter une étude numérique de la micro-fissuration induite par le retrait dans les structures en béton. La méthode numérique utilisée est basée sur la périodynamique (PD). Dans un premier temps, un modèle numérique composé une matrice cimentaire endommageable et les granulats élastiques est construit. Les granulats sont distribués régulièrement dans la matrice. Une série des études paramétriques ont été réalisées afin d'étudier l'influence du taille et de la fraction volumétrique des garnulats. Les largeur des fissures obtenus dans les différents cas sont comparées. En se basant sur les résultats obtenus, un modèle numérique avec une distribution aléatoire des granulats est ensuite proposé. Enfin, les résultats numériques sont comparés avec les observations expérimentales et une bonne concordance est obtenue.*

## Abstract :

*This work presents a numerical investigation of shrinkage induced micro-cracking of concrete by using the peridynamics theory. A numerical concrete model, with a regular aggregate arrangements, is firstly established. In order to study the influence of the aggregate diameter as well as its volume fraction, a series of parametric studied has been performed. The obtained value of crack width have been compared. Based on the previous results, a new numerical model with random aggregate arrangements is proposed for studied material. Finally, the numerical prediction is compared with the experimental investigation. The results show that a good agreement is obtained between the numerical results and experimental observations.*

**Mots clefs : Peridynamics/ Shrinkage/ Micro-cracking/ Concrete/ Numerical analysis**

## Nomenclature

$\rho$	mass density of material point
$\mathbf{f}$	pairwise force between two material points connected by a bond
$\mathbf{x}, \mathbf{x}'$	location vector of material point
$\ddot{\mathbf{u}}$	acceleration vector of material point
$t$	time step
$H_x$	horizon of material point $x$
$V'$	volume of material point $x'$
$\mathbf{b}$	body force density
$\delta$	horizon size
$B$	body of model
$s$	stretch of a bond
$\boldsymbol{\xi}$	relative position vector of two material points
$\boldsymbol{\eta}$	relative displacement vector of two material points
$\omega$	micro-potential
$c$	micro-modulus function denoting the stiffness of a pairwise bond
$g$	kernel function describes the spatial distribution of intensity of long-range forces in materials
$E$	Young's modulus of the solid
$h$	thickness of structure model
$\mu$	scalar function describes the state of the bond
$s_0$	critical stretch for bonds
$G_0$	macroscopic fracture energy
$\psi$	local damage of material point $\mathbf{x}$
$n$	time step instant
$V_j$	volume of material point $j$ involved in the horizon of point $i$
$\Delta x$	element size of the model
$G_{ij}$	surface correction factor between point $i$ and $j$
$C_{v_j}$	volume correction factor for point $j$ related to point $i$
$\mathbf{M}$	fictitious diagonal density coefficient matrix for time integration
$d_c^n$	damping coefficient
$\mathbf{F}$	pairwise force between two material points connected by a bond for time integration
$\Delta t$	time step size
$\mathbf{K}^n$	diagonal "local" stiffness matrix
$\lambda_{ii}$	entries on the main diagonal of $\mathbf{M}$
$C$	the maximum value of $c$
$L$	the length of the specimen
$\phi$	diameter of the aggregates
$\rho$	volume fraction of the model
$G_{ft}$	macroscopic fracture energy of tension
$G_{fc}$	macroscopic fracture energy of compression
$\nu$	Poisson's ratio of solids
$l_i$	length of the element of the model
$H_i$	length of a bond initial of two points connected directly
$\varepsilon$	shrinkage strain

## Introduction

Concrete is widely used in engineering structures. During the lifetime of structures, it is submitted to various coupled conditions such as mechanical loading, desaturation and re-saturation, temperature variation and chemical degradation. In order to guarantee the durability of structures, it is necessary to identify the mechanical behavior of concrete under multi-field stress conditions. The drying process leads to desiccation shrinkage of cement paste. This drying shrinkage due to moisture gradients between the surface and core of the structure is prevented by a structural effect, which can induce surface micro-cracking. Moreover, it can be restrained by the aggregates due to the stiffness difference between aggregates and cement paste, which leads to radial and bond micro-cracking. Cement-based materials thus can be damaged without any direct mechanical loading, such as loss of concrete stiffness and strength, increase of permeability, etc. The present study is focused on the evolution of shrinkage cracking in cement-based materials. However, in a normal concrete, due to the great variability of aggregate (shape, size distribution and porosity, etc.) and the eventual reaction between the cement matrix and the inclusions, it is very difficult to analyze the mechanisms controlling the creation and development of cracks. Simulation of the failure in solid materials is one of the major concerns in engineering science and solid mechanics. Due to the demand of simulating crack initiation and propagation process in solid materials, different methods have been developed. In the framework of continuum mechanics, several methods (for instance : the finite element method (FEM) [1], the finite difference method (FDM) [2]) have been proposed. However, they exhibit high mesh dependence. In view of this, the meshless methods are introduced. But their high-order continuous approximation functions used cannot provide a good prediction of crack propagation. Therefore, the extended finite element method (XFEM) [3] and the discrete finite element method (DFEM) [4], are proposed. In these two methods, additional functions are introduced to describe the discontinuous mechanical problems. They are still incapable of analyzing the complex propagation of cracks and fissures in three-dimensional group.

On the other hand, the peridynamics method (PD) [5] can provide a good description of development and propagation of cracks/fissures. Because in PD theory, the studied structure is divided into a series of material points, which satisfy all the physical law. In other words, it's a non-local theory of solid mechanics, based on integral equilibrium equations. Therefore, the basic equilibrium equation of a material point is verified by using the integral of internal forces exerted on non-adjacent points over a finite distance. This non-local model is mathematically compatible with the initiation and propagation of cracks, since integral equations could naturally handle discontinuities. In addition, the peridynamics can solve both the static and dynamic problems.

In this work, a numerical study of shrinkage micro-cracking in concrete has been presented by using the peridynamics theory. In view of this, the numerical model of studied concrete, with a regular aggregate arrangements, is firstly formulated. In order to study the influence of the aggregate diameter and its volume fraction, a series of parametric studies have been performed. The average crack width in different cases are compared. Based on obtained numerical results, a second numerical model with random aggregate arrangements is proposed. Finally, the numerical prediction will be compared with the experimental investigation.

## The peridynamics formulation for micro-elastic materials

The non-local continuum theory peridynamics is firstly introduced by Silling in [5]. And it is introduced to describe the mechanical behaviors in continuum media by using an integral of forces instead of

divergence of stress. Each pair of particles interacts via a vector function  $\mathbf{f}$ , basing the position  $\mathbf{x}$  and the displacement  $\mathbf{u}$  to the reference point, called a pairwise force function, as shown in Figure 1. The peridynamics (PD) equation of motion at a material point  $\mathbf{x}$  and the time  $t$  according to the Newton's law is given as[6] :

$$\rho(\mathbf{x})\ddot{\mathbf{u}}(\mathbf{x}, t) = \int_{H_x} \mathbf{f}(\mathbf{x}, \mathbf{x}', \mathbf{u}(\mathbf{x}, t), \mathbf{u}(\mathbf{x}', t), t) dV' + \mathbf{b}(\mathbf{x}, t) \quad (1)$$

where  $\rho$  is the mass density of material particle,  $\mathbf{u}$  is the displacement vector field,  $\mathbf{b}$  is the prescribed loading force density field which represents the external force per unit reference volume,  $H_x$  is the neighborhood of material particle  $\mathbf{x}$  within his horizon size  $\delta$ , which is usually taken to be a sphere in 3D or a circle in 2D problems centered of  $\mathbf{x}$ , and given as :

$$H_x = H(\mathbf{x}, \delta) = \{\mathbf{x}' \in B : \|\mathbf{x}' - \mathbf{x}\| \leq \delta\} \quad (2)$$

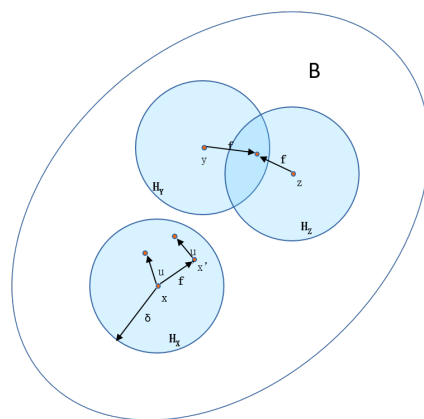


Fig. 1: interactions between the points material

$\mathbf{f}$  can be simplified as  $\mathbf{f}(\boldsymbol{\eta}, \boldsymbol{\xi})$ , with relative position of two particles in the reference configuration  $\boldsymbol{\xi} : \boldsymbol{\xi} = \mathbf{x}' - \mathbf{x}$ , and their relative displacement  $\boldsymbol{\eta} : \boldsymbol{\eta} = \mathbf{u}' - \mathbf{u}$ . And  $\mathbf{f}(\boldsymbol{\eta}, \boldsymbol{\xi}) = 0$  when  $\|\boldsymbol{\xi}\| > \delta$ .

And the normal deformation (stretch)  $s$  of a bond can be defined as

$$s = \frac{\|\boldsymbol{\eta} + \boldsymbol{\xi}\| - \|\boldsymbol{\xi}\|}{\|\boldsymbol{\xi}\|} \quad (3)$$

For the micro-elastic material[5][6], the pairwise force function  $\mathbf{f}$  is derivable from a scalar micro-potential  $\omega(\boldsymbol{\eta}, \boldsymbol{\xi}) = \frac{c(\boldsymbol{\xi}, \delta) s^2 \boldsymbol{\xi}}{2}$ , then  $\mathbf{f}$  can be expressed as

$$f(\boldsymbol{\eta}, \boldsymbol{\xi}) = \begin{cases} \frac{\partial \omega(\boldsymbol{\eta}, \boldsymbol{\xi})}{\partial \boldsymbol{\eta}} = \frac{\boldsymbol{\eta} + \boldsymbol{\xi}}{\|\boldsymbol{\eta} + \boldsymbol{\xi}\|} sc(\boldsymbol{\xi}, \delta) & \text{when } \|\boldsymbol{\xi}\| \leq \delta \\ 0 & \text{else} \end{cases} \quad (4)$$

where  $c(\boldsymbol{\xi}, \delta) = c(0, \delta)g(\boldsymbol{\xi}, \delta)$  is the micro-modulus function denoting the stiffness of a pairwise bond, and the kernel function  $g(\boldsymbol{\xi}, \delta)$  describes the spatial distribution of intensity of long-range forces in materials. According to Huang et al.[7][8], the micro-modulus  $c$  should gradually get weaker with the length of bond  $\boldsymbol{\xi} = \|\boldsymbol{\xi}\|$  increases, and it vanishes when their length of bond reaches the horizon  $\delta$ . So,

the micro-modulus in 2D problems can be given by :

$$c(\boldsymbol{\xi}, \delta) = \begin{cases} \frac{315E}{8\pi h\delta^3} \left[1 - \left(\frac{\|\boldsymbol{\xi}\|}{\delta}\right)^2\right]^2 & \text{when } \|\boldsymbol{\xi}\| \leq \delta \\ 0 & \text{else} \end{cases} \quad (5)$$

where  $h$  is the thickness of structure model and  $E$  is the Young's model of the solid, and the effective Poisson's ratio is limited to 1/3 here for the plane stress situation[9]. Damage can be incorporated into the PD constitutive model by allowing the bonds for solid interactions to break irreversibly. And taking the bond-broken into the consideration, the force can be modified through a history-dependent scalar-valued function  $\mu(\boldsymbol{\xi}, \mathbf{x}, t)$ ,

$$\mu(\boldsymbol{\xi}, \mathbf{x}, t) = \begin{cases} 1, & \text{whens } \leq s_0 \\ 0, & \text{whens } > s_0 \end{cases} \quad (6)$$

where  $s_0$  is the critical stretch for bonds. It is related to the macroscopic fracture energy  $G_0$  which is experimental measurable. By following the same procedure performed in [6][10][11] for the plane stress bond-based PD analysis,  $G_0$  is :

$$G_0 = 2h \int_0^\delta \left\{ \int_z^\delta \int_0^{\cos^{-1} Z/\xi} \frac{cs_0^2 \xi^2}{2} d\phi d\xi dz \right\} \quad (7)$$

By combining the Eq.5 and Eq.7,  $G_0$  finally writes as :

$$G_0 \approx \frac{8E\delta s_0^2}{5\pi} \quad (8)$$

So the critical stretch of bonds  $s_0$  is

$$s_0 = \sqrt{\frac{5\pi G_0}{8E\delta}} \quad (9)$$

Then the pairwise force function can be modified as

$$f(\boldsymbol{\eta}, \boldsymbol{\xi}) = \begin{cases} \frac{\partial \omega(\boldsymbol{\eta}, \boldsymbol{\xi})}{\partial \boldsymbol{\eta}} = \frac{\boldsymbol{\eta} + \boldsymbol{\xi}}{\|\boldsymbol{\eta} + \boldsymbol{\xi}\|} sc(\boldsymbol{\xi}, \delta) \mu(\boldsymbol{\xi}, \mathbf{x}, t) & \text{when } \|\boldsymbol{\xi}\| \leq \delta \quad \text{and} \quad s < s_0 \\ 0 & \text{else} \end{cases} \quad (10)$$

According to this criterion for damage, Silling[6][13] and Kilic[12][14] give the local damage at the  $\mathbf{x}$  point in the material as

$$\psi(\mathbf{x}, t) = 1 - \frac{\int_{H_x} \mu(\mathbf{x}, \boldsymbol{\xi}, t) dV'_x}{\int_{H_x} dV'_x} \quad (11)$$

where  $V'_x$  is the volume of the  $\mathbf{x}'$  point.

## Numerical implementation

### Spatial discretization and correction

The region is discretized into nodes (material particles), each with a known volume in the reference configuration. And in this study, the sample is discretized into particles with the uniform grid spacing configuration. The horizon is chosen as  $\delta = 3.015\Delta x$ , which is slightly greater than  $3\Delta x$  commonly used in PD model[6] for the case of coarsest grid studied, and the  $\Delta x$  is the element size of the model.

Then the spatial integration in PD is converted into a summation of finite number of material lattices,

$$\rho \ddot{\mathbf{u}}_i^n = \sum_{j=1}^{N_{Hx_i}} G_{ij} \mathbf{f}(\mathbf{u}_j^n - \mathbf{u}_i^n, \mathbf{x}_j - \mathbf{x}_i) C_{v_j} V_j + \mathbf{b}_i^n \quad (12)$$

where  $n$  is the time step number, and subscripts denote the node number, so that  $\ddot{\mathbf{u}}_i^n = \mathbf{u}(\mathbf{x}_i, t^n)$ .  $V_j$  is the volume of point  $j$  involved in the horizon of point  $i$ , in 2D problems,  $V_j = \Delta x^2 * h$ .

$G_{ij}$  is the surface correction factor, it is introduced for the material points closed to free surfaces or material interfaces, as shown in Figure 2. It is related to the relative position of particle  $i$  and  $j$  and ratio of the deformation energy density of the material in classical continuum mechanical method and PD method [10][15].

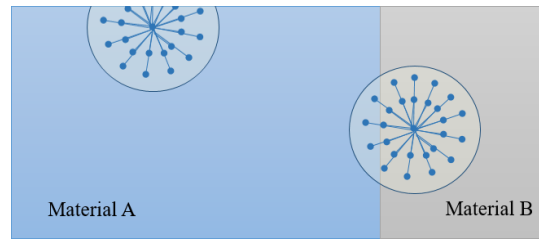


Fig. 2: Surface effect of the points near the boundary and interfaces

$C_{v_j}$  is the volume correction factor. As illustrated in Figure 3, the material points near the boundary is partly belong to the horizon. So it is necessary to correct the volume fraction for the points in summation, the volume correction factor is expressed as

$$C_{v_j} = \begin{cases} 0 & \text{when } \|\boldsymbol{\xi} + \boldsymbol{\eta}\| \geq \delta \\ 1 & \text{when } \|\boldsymbol{\xi} + \boldsymbol{\eta}\| \leq (\delta - r) \\ \left(\frac{\delta + r - \|\boldsymbol{\xi} + \boldsymbol{\eta}\|}{2r}\right) & \text{when } (\delta - r) \leq \|\boldsymbol{\xi} + \boldsymbol{\eta}\| \leq \delta \end{cases} \quad (13)$$

where  $r = \frac{\Delta x}{2}$ .

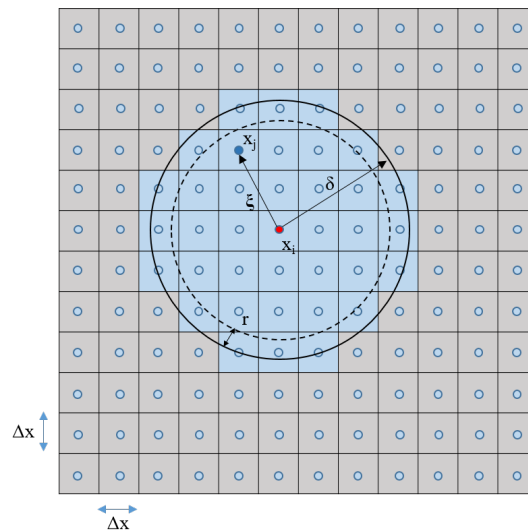


Fig. 3: Volume correction for the collocation points inside the horizon

## Time integration

For this study, an adaptive dynamic relaxation method is used, which is introduced by Kilic and Madenci[16]. According to the ADR method, the PD equation of motion is written as a set of ordinary differential equations for all material points in the system by introducing a damping coefficient  $d_c^n$  [17] and a fictitious diagonal density coefficient matrix  $\mathbf{M}$ .

$$\mathbf{M}\ddot{\mathbf{U}}^n(\mathbf{X}, t) + d_c^n \mathbf{M}\dot{\mathbf{U}}^n(\mathbf{X}, t) = \mathbf{F}^n(\mathbf{U}, \mathbf{U}', \mathbf{X}, \mathbf{X}') \quad (14)$$

By utilizing central-difference explicit integration, displacements and velocities for the next time step can be obtained as

$$\dot{\mathbf{U}}^{n+1/2} = \frac{(2 - d_c^n \Delta t)\dot{\mathbf{U}}^{n-1/2} + 2\Delta t \mathbf{M}^{-1} \mathbf{F}^n}{2 + d_c^n \Delta t} \quad (15)$$

and

$$\mathbf{U}^{n+1} = \mathbf{U}^n + \Delta t \dot{\mathbf{U}}^{n+1/2} \quad (16)$$

By assuming that  $\mathbf{U}^0 \neq 0$  and  $\dot{\mathbf{U}}^{-1/2} = 0$ , the integration started by

$$\dot{\mathbf{U}}^{1/2} = \frac{\Delta t \mathbf{M}^{-1} \mathbf{F}^0}{2} \quad (17)$$

where  $\Delta t$  is the time step, it do not have to be physical quantities, in dynamic relaxation, a time step size of 1 ( $\Delta t = 1$ ) is a common choice. According to Madenci and Oterkus[10], the damping coefficient  $d_c^n$  in 2D context can be expressed as

$$d_c^n = 2\sqrt{\frac{(\mathbf{U}^n)^T \mathbf{K}^n \mathbf{U}^n}{(\mathbf{U}^n)^T \mathbf{U}^n}} \quad (18)$$

where  $\mathbf{K}^n$  is the diagonal "local" stiffness matrix, which is given as

$$K_{ii}^n = \frac{F_i^n - F_i^{n-1}}{\lambda_{ii} \Delta t \dot{u}_i^{t-1/2}} \quad (19)$$

with the entries on the main diagonal of  $\mathbf{M}$ ,

$$\lambda_{ii} = \frac{\pi \delta^2 h C \Delta t^2}{4 \Delta x} \quad (20)$$

where  $C$  takes the maximum value of Eq.5.

## Numerical analysis of shrinkage induced micro-cracking

Shrinkage induced micro-cracking was analyzed by means of the PD approach described above. The elements representing the cement paste were subjected to an incrementally applied uniform shrinkage strain of bonds up to  $\varepsilon = 0.5\%$ . This value was chosen for the simulation to represent a relatively severe shrinkage of neat cement paste on first-drying shrinkage. The influence of aggregate volume fraction and aggregate diameter was studied. Aggregate volume fractions  $\rho = 0.5, 0.3$  and  $0.1$  were modeled. Furthermore, four different aggregate diameters  $\phi = 16, 8, 4$  and  $2mm$  were used. The geometry of the specimen analyzed for all volume fractions and aggregate sizes is shown in Figure 4, and the same detail

of discretization was applied with  $\Delta x = 0.25mm$ . The length  $L$  of the specimen is

$$L = \sqrt{\frac{\pi\phi^2}{\rho}} \quad (21)$$

The material parameters for the constitutive model were chosen according to Table 1. For an aggregate

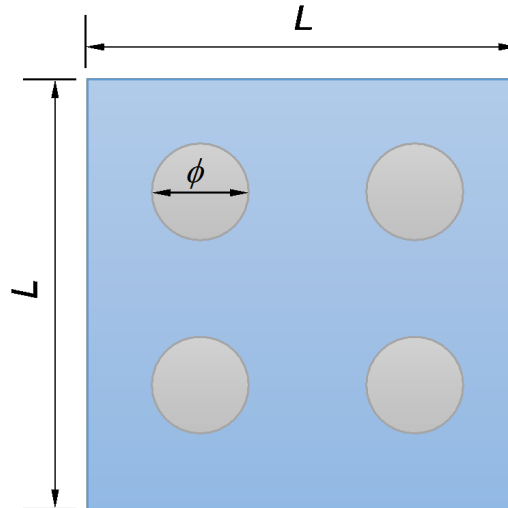


Fig. 4: Numerical model

Material	$E[GPa]$	$G_{ft}[J/m^2]$	$G_{fc}[J/m^2]$	$\nu$
Cement Paste	40	100	100,000	1/3
Aggregate	100	-	-	1/3

TABLE 1: Material parameters for the constitutive model

diameter  $\phi = 16mm$  and the volume fraction  $\rho = 0.3$ , the damage pattern is shown in Figure 5. Generally, some bond cracks between the aggregate and paste can be observed, however most cracks appear to originate at the aggregate surface and propagate towards the matrix. When the cement was subjected to drying shrinkage, the cracks were seen to occur near the shortest distance between aggregates and connect them soon in a regular square pattern, which is similar with the pattern in the research of Grassl et al. [18].

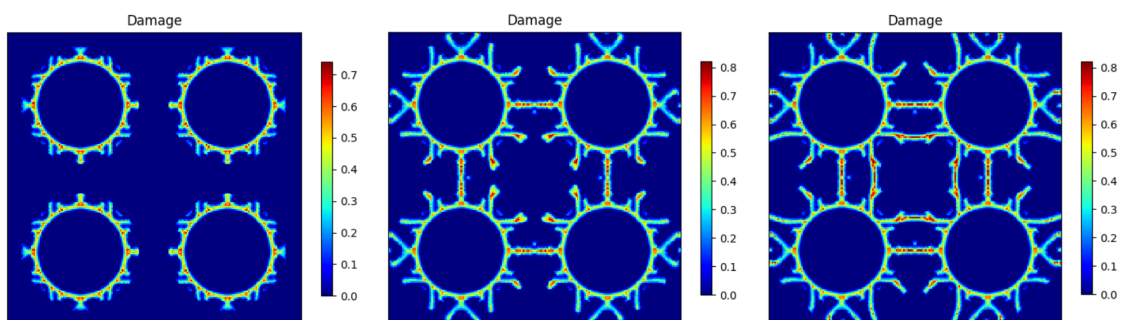


Fig. 5: Crack evaluation for  $\rho = 0.3$  and  $\phi = 16mm$

Width of micro-cracks for different volume fractions and aggregate diameters were compared. Inspired by Grassl et al.[18], The average crack width is

$$w_c = \frac{\sum_{i=1}^{n_c} l_i H_i s_i}{\sum_{i=1}^{n_c} l_i} \quad (22)$$

where  $l_i$  is the length of element, so that  $l_i = \Delta x$  for these model with a uniform discretization,  $n_c$  is the number of cracked elements. Recall that  $s$  is the stretch of a bond, and  $H$  is the length of a bond initial of two elements connected directly, so that  $H = \Delta x$ .

The influence of the aggregate diameter and volume fraction on the average crack width is shown in Figure 6. The average crack width decreases with decreasing aggregate size at constant volume fraction. An increase of volume fraction at constant aggregate size results in a decrease of crack width.

Figure 7 shows the crack pattern for  $\rho = 0.3$  for  $\phi = 8mm$  at a shrinkage strain in the matrix of

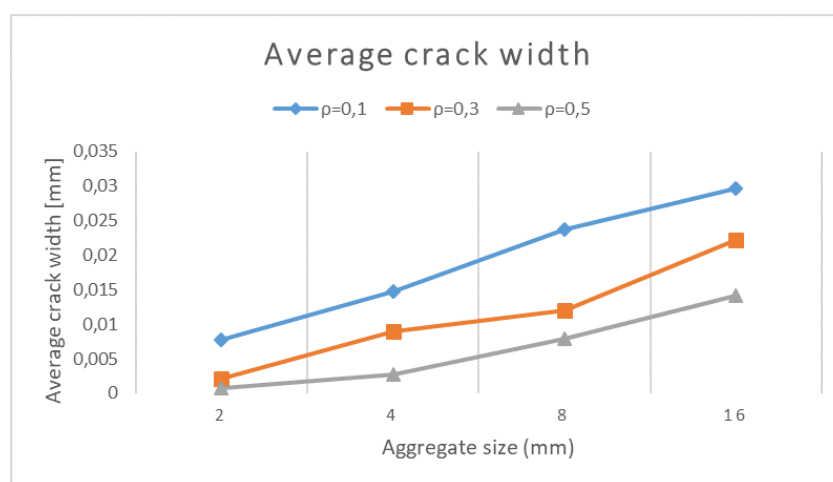


Fig. 6: Average crack width  $w_c$

$\varepsilon = 0.5\%$  at a random arrange of aggregate. The partial bond cracks appearing around some aggregate particles and the matrix cracks that propagate through the paste and very often bridging several aggregate particles. And it is similar to the crack pattern in the research experimental of Rougelot [19], as illustrate in Figure 8. It can be seen that the numerical simulation results of the entire process of failure are consistent with the experimental results. Numerical simulations of this classical example do not require any external failure criteria, and it shows that the PD method has a great advantage in simulating fracture.

## Conclusion

In the present work, the influence of size and volume fraction of aggregate on shrinkage induced micro-cracking was studied numerically by using the PD method. The obtained results show that the average crack width increases with the aggregate diameter and decreases with the volume fraction of aggregate. And the creation and propagation of fissures are satisfactorily by the numerical simulations.

Although a good agreement is generally obtained between the numerical simulations and the experimental observations, the representation of aggregates approximation and size selection are oversimplified in the present study. Therefore, the future work will improve the modeling method to make it more realistic models and extend the modeling approach to 3D.

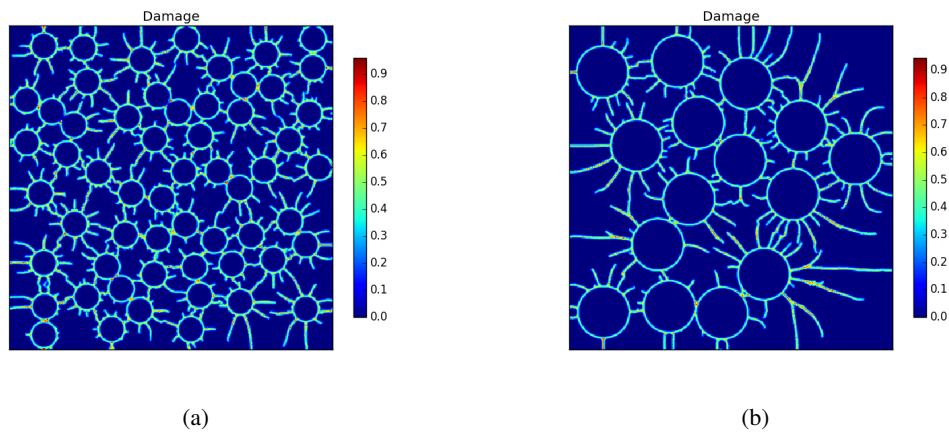


Fig. 7: Crack patterns for (a)  $\rho = 4\text{mm}$  and (b)  $\rho = 8\text{mm}$  at a shrinkage strain in the matrix of  $\varepsilon = 0.5\%$

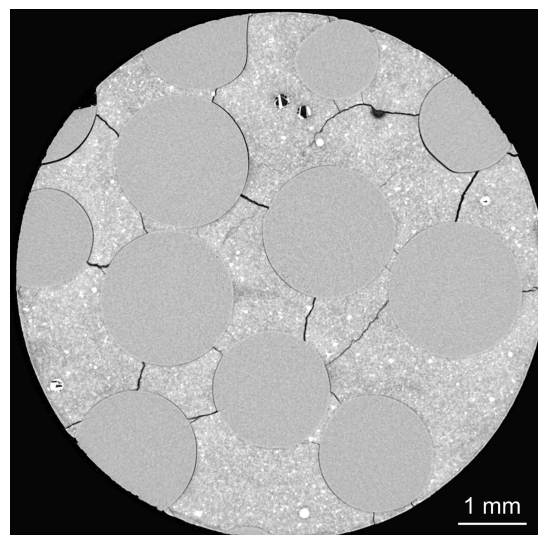


Fig. 8: Micro-tomographic slice of a composite *C2* after 48 hours of drying[19]

## Références

- [1] Arne Hillerborg, Mats Modéer, and P-E Petersson. Analysis of crack formation and crack growth in concrete by means of fracture mechanics and finite elements.
- [2] T. Liszka and J. Orkisz. The finite difference method at arbitrary irregular grids and its application in applied mechanics. *Computers & Structures*, 11(1) :83–95, 1980.
- [3] Nicolas Moës, John Dolbow, and Ted Belytschko. A finite element method for crack growth without remeshing. *International journal for numerical methods in engineering*, 46(1) :131–150, 1999.
- [4] E. Oñate and J. Rojek. Combination of discrete element and finite element methods for dynamic analysis of geomechanics problems. *Computer Methods in Applied Mechanics & Engineering*, 193(27) :3087–3128, 2004.  
*Cement and concrete research*, 6(6) :773–781, 1976.
- [5] Stewart A Silling. Reformulation of elasticity theory for discontinuities and long-range forces. *Journal of the Mechanics and Physics of Solids*, 48(1) :175–209, 2000.
- [6] Stewart A Silling and Ebrahim Askari. A meshfree method based on the peridynamic model of solid mechanics. *Computers & structures*, 83(17-18) :1526–1535, 2005.
- [7] Dan Huang, Guangda Lu, and Pizhong Qiao. An improved peridynamic approach for quasi-static elastic deformation and brittle fracture analysis. *International Journal of Mechanical Sciences*, 94 :111–122, 2015.
- [8] Dan Huang, Guangda Lu, Chongwen Wang, and Pizhong Qiao. An extended peridynamic approach for deformation and fracture analysis. *Engineering Fracture Mechanics*, 141 :196–211, 2015.
- [9] Walter Gerstle, Nicolas Sau, and Stewart Silling. Peridynamic modeling of plain and reinforced concrete structures. 2005.
- [10] Erdogan Madenci and Erkan Oterkus. *Peridynamic theory and its applications*, volume 17. Springer, 2014.
- [11] Tao Ni, Qi-zhi Zhu, Lun-Yang Zhao, and Peng-Fei Li. Peridynamic simulation of fracture in quasi brittle solids using irregular finite element mesh. *Engineering Fracture Mechanics*, 188 :320–343, 2018.
- [12] Bahattin Kilic. *Peridynamic Theory for Progressive Failure Prediction in Homogeneous and Heterogeneous Materials*. PhD thesis, The University of Arizona, 2008.
- [13] Richard W Macek and Stewart A Silling. Peridynamics via finite element analysis. *Finite Elements in Analysis and Design*, 43(15) :1169–1178, 2007.
- [14] B. Kilic and E. Madenci. Structural stability and failure analysis using peridynamic theory. *International Journal of Non-Linear Mechanics*, 44(8) :845 – 854, 2009.
- [15] Q. V. Le and F. Bobaru. Surface corrections for peridynamic models in elasticity and fracture. *Computational Mechanics*, 61(4) :499–518, apr 2018.
- [16] B. Kilic and E. Madenci. An adaptive dynamic relaxation method for quasi-static simulations using the peridynamic theory. *Theoretical & Applied Fracture Mechanics*, 53(3) :194–204, 2010.
- [17] P Underwood. *Dynamic relaxation, Ch. 5 in Computational methods for transient analysis (edited by Belytschko T. and Hughes TJ R)*. Elsevier Science Publishers, 1983.

- [18] Peter Grassl, S. Wong Hong, and Nick R. Buenfeld. Influence of aggregate size and volume fraction on shrinkage induced micro-cracking of concrete and mortar. *Cement & Concrete Research*, 40(1) :85–93, 2010.
- [19] Thomas Rougelot, Cheng Peng, Nicolas Burlion, and Dominique Bernard. Why is it necessary to use a damage model to simulate the mechanical behavior of concrete under drying and leaching ? *Revue Française De Génie Civil*, 14(6-7) :923–935, 2010.